TDA Progress Report 42-96 October–December 1988

Systems Analysis for DSN Microwave Antenna Holography

D. J. Rochblatt
Radio Frequency and Microwave Subsystems Section

~~This article analyzes~~ proposed systems for Deep Space Network (DSN) microwave antenna holography. Microwave holography, as applied to antennas, is a technique which utilizes the Fourier Transform relation between the complex far-field radiation pattern of an antenna and the complex aperture field distribution to provide a methodology for the analysis and evaluation of antenna performance. Resulting aperture phase and amplitude distribution data are used to precisely characterize various crucial performance parameters, including panel alignment, subreflector position, antenna aperture illumination, directivity at various frequencies, and gravity deformation. Microwave holographic analysis provides diagnostic capacity as well as, perhaps more significantly, a powerful tool for evaluating antenna design specifications and their corresponding theoretical models. Functional requirements, performance, and potential for future technological growth are considered, leading to a description of complete in-house DSN capability for operational "health checks," evaluations, diagnostics, and performance optimization, as well as a flexible R&D tool for further development of large antennas. Wide-bandwidth, narrow-bandwidth, and phase-retrieval systems are analyzed and discussed with respect to three relevant signal sources: a natural radio star, a satellite channel of perhaps telephone or computer data that can be treated as a Gaussian noise source, and a satellite CW beacon. A recommendation based on systems analysis is made to first implement the narrow-bandwidth CW system. It will provide high-resolution and low-resolution holographic maps with high precision suitable for individual panel setting, and function as a flexible R&D engineering tool offering future growth potential. With modest software addition, a wide-bandwidth 1-bit correlator could become part of that system, providing low-resolution maps in the DSN frequency bands that satisfy the requirement for a quick response to operational needs. Since the implementation of 1-bit correlators in the DSN stations is not envisioned before 1994, and since DSN Operations desires a low-cost implementation of quick "health check" diagnostic capabilities as soon as possible, it is recommended that a phase-retrieval-based holography system be developed for that purpose.

I. Introduction

Microwave antenna holography implementation for the DSN must satisfy at least three primary requirements. First, it must satisfy DSN Operations' need for a quick "health check" of the antenna mechanical and microwave subsystems to yield an unambiguous go/no go operational antenna status result. The holography measurement must be conducted within the DSN frequency bands using the operational microwave front-end equipment. To derive the required quantitative parameters, holographic maps of low resolution and medium accuracy are sufficient. The measurement time needed for these maps is

about 30 minutes, and will be conducted by antenna operators using transferred hardware and software.

Second, the system must satisfy DSN Operations' implementation needs for accurate reflector panel setting adjustments. To derive the required quantitative parameters, holographic maps of high resolution and high precision are needed. To complete the data acquisition measurement for these maps, 12 hours are needed for the 70-m antennas and 6 hours for the 34-m antennas. It is recommended that the holography system chosen promise future reduction in measurement time as stronger signal sources become available. This panel setting mode is not expected to be used frequently. Therefore, a special test equipment mode of operation by a station engineer/analyst could be used. The data processing and detailed diagnostics of the data need not be the responsibility of station personnel and might be done at JPL.

Third, a DSN microwave holography system must provide future technological growth potential in terms of measurement precision, data acquisition speed, and in understanding the performance limitations of large, efficient microwave reflector antennas for deep space communications. Microwave holography will provide a major tool in future studies of understanding a broad range of factors that affect antenna performance, including: reflector panel manufacturing; setting precision; beam pointing; focus; gain; phase stabilities; mechanical hysteresis; and weather, paint, aging, thermal, and wind effects.

The measurement system selected must support the DSN's need to acquire every 0.1-dB gain improvement available from its major antennas, and must also support the operational need for a quick "health check," including first-order evaluations of the mechanical antenna and microwave front end.

The operational measurement system must be compatible with the antenna operational configuration. Both conventional and beam waveguide 32-GHz antennas must be supported. The use of non-DSN frequencies, feeds, or amplifiers/receivers should be minimized or eliminated if possible. Commercial equipment that includes manufacturer support for a 10-year period must be carefully selected.

II. Requirements Summary

The parameters critical for the quality of the images derived from holographic measurements are signal-to-noise ratio (SNR), instrumentation dynamic range, and overall measurement system accuracy. A detailed mathematical derivation of the related equations can be found in [1–3].

In the first "health check" mode of operation, a lateral resolution of typically D/20 is necessary, which can be achieved with a data array size of 25 X 25. The standard deviation of the image error profile need be no better than $\lambda/100$, and optimum subreflector settings need be no better than $\lambda/10$ at 8 GHz. When the antenna scan rate traverses a sidelobe per second and allows sample smearing of 5 to 10 percent, an integration time of 0.1 sec is indicated. Under the above conditions, it will take 30 minutes to produce a 25 X 25 array. To achieve image quality with a standard deviation of 0.5 mm on the 70-m or 34-m antennas with lateral resolutions of D/20, an approximate beam-peak SNR of 45 dB (in an integration period of 0.1 sec) is required at X-band (8.4 GHz), or 42 dB at Ku-band (11.45 GHz). (To achieve the same specifications with phase-retrieval holography, as described in Section IV, an approximate beam-peak SNR of 60 dB is required at S-band [2.2 GHz].)

In the second panel-setting mode, the large number of individual panels (each with an area of 2 m^2) on the 70-m and 34-m antennas (arranged in 17 and 9 circumferential rings, respectively) dictates a high lateral resolution of about 0.35 m. Array data sizes of 197 X 197 and 127 X 127 for the 70-m and 34-m antennas, respectively, are necessary. The two-dimensional far-field pattern must be sampled out to approximately the 90th (60th) sidelobe for the 70-m (34-m) antenna to provide the required resolution. Since the antenna far-field radiation pattern falls off rapidly away from beam peak, a specification of system dynamic range greater than 80 dB is necessary for measurement to the 90th sidelobe. For a maximum of 0.1-dB degradation in antenna efficiency due to random surface imperfections, the rms surface error must be no greater than 0.012λ. This translates to an rms surface error of 0.43 mm at X-band (8.4 GHz) and 0.11 mm at Ka-band (32 GHz). To achieve surface error maps with one standard deviation of 0.1 mm at resolution cell size of 0.35 m for the 70-m antenna, a beam-peak SNR of 73 dB is required at Ku-band (11.45 GHz) and 75 dB at X-band (8.4 GHz). On the average, there are 25 data points on each panel, which provide screw adjustment accuracy of 0.02 mm. Theoretically, one calculates that an 87-dB SNR would be required at S-band (2.2 GHz). However, diffraction effects at this frequency contaminate the holographic images, making the data unsuitable for precise panel setting. To achieve the same accuracy on the 34-m antenna, a beam-peak SNR of 66 dB is required at Ku-band and 69 dB at X-band [3]. The accuracy of the subreflector position correction will typically be 0.5 mm.

The accuracy across holographic maps varies with the aperture amplitude taper illumination. Results are better at the center of the dish and gradually become worse toward the edge of the dish. For a uniformly illuminated dish, accuracy stays relatively constant through most of the dish and becomes quickly worse just at the edge where the illumination falls off

rapidly. The values calculated here are at the position of average amplitude taper value.

Antenna scan rates, signal SNR, signal source orbit stability, integration time, and sample smearing constraints lead to a 12-hour (presently nighttime) measurement time for the 70-m antenna (6 hours for the 34-m antenna) to obtain the high-resolution high-precision maps. A decrease in measurement time is desirable and can only be achieved with a receiver system compatible with the signal source. Such a system will provide higher SNR at shorter integration time periods as stronger signal sources become available. The narrow-bandwidth system matched to satellite CW signals can provide this future capability. This will allow low-resolution (25 X 25) image data acquisition in approximately 15 minutes. Meaningful wind and thermal information, for example, would become available for the first time with such fast imaging capture. Additional system requirements include antenna pointing precision of ±0.002 deg and angle encoder sampling intervals of 10 msec.

III. Systems Analysis

A. Wide-Bandwidth System

For the implementation of the 1-bit A/D and the 1-bit correlator for holographic measurements, three cases must be considered, as in each, the 1-bit correlator operates differently:

Case I: Weak signal—either a CW or Gaussian noise source

Case II: Strong CW signal

Case III: Strong Gaussian noise source

For two antennas with system temperatures T_{s1} and T_{s2}, which are pointed at a source giving antenna temperatures T_{a1} and T_{a2}, with channel bandwidth B (Hz) and an integration period of T (sec), the SNR of the correlated fringe amplitude to rms noise is

$$SNR = \eta \sqrt{\left[\frac{T_{a1}\, T_{a2}}{(T_{s1} + T_{a1})(T_{s2} + T_{a2})}\right][2BT]} \qquad (1)$$

where η is a factor accounting for losses due to quantization and processing. The loss factors are multiplicative, so the total loss is given by

$$\eta = \eta_Q\, \eta_R\, \eta_S\, \eta_D \qquad (2)$$

where

η_Q = quantization loss for 1 bit, two-level is $2/\pi$ (0.637)

η_R = fringe rotation loss for three-level, one path is 0.960

η_S = loss due to fringe counter rotation, one channel is 0.707 ($1/\sqrt{2}$)

η_D = discrete delay step loss, which for spectral correction is 1.00

Conservatively, $\eta = 0.432$ (–7.3 dB).

For Case I, $T_{ai} \ll T_{si}$, and the SNR (Eq. 1) can be reduced to

$$SNR_I = 0.43 \sqrt{\left[\frac{T_{a1}\, T_{a2}}{T_{s1}\, T_{s2}}\right][2BT]} \qquad (3)$$

For Cases II and III, $T_{ai} \gg T_{si}$, and the SNR equation becomes

$$SNR_{II,III} = 0.43\sqrt{2BT} \qquad (4)$$

and is independent of the size of the antennas because the SNR is determined by the fluctuations in signal level. That is the saturated condition [4].

Only when a 1-bit correlator is operating under Case I conditions (Eq. 3) can it provide accurate amplitude and phase measurements. When the correlator is operating under Case II or III, it can no longer provide amplitude measurements, as the correlation (ρ) is equal to a constant equal to 1:

$$\rho_{T_{ai} \gg T_{si}} = \sqrt{\frac{T_{a1}\, T_{a2}}{(T_{s1} + T_{a1})(T_{a2} + T_{s2})}} = 1 \qquad (5)$$

However, it can still provide accurate phase measurement if the observable is a Gaussian noise source. If the observable is a CW signal, neither accurate phase nor amplitude measurement can be obtained (assuming Nyquist sampling rate)[1] [5, 6]. It can be shown[2] that for a sinusoidal signal $y(t)$ buried in Gaussian noise $n(t)$ which has a normalized probability density function

$$G(x) = \frac{1}{\sqrt{2\pi}} \exp\left[\frac{-x^2}{2}\right] \qquad (6)$$

[1] E. H. Sigman, "Phase Measurement of Sinusoidal Tones Buried in Noise," JPL Engineering Memorandum 315-74 (internal document), November 1978.

[2] Ibid.

with standard deviation $\sigma = 1$, the detected signal at a particular time t_1 at the output of a 1-bit A/D converter is

$$d(t_1) = \frac{2N}{\sqrt{2\pi}}\left[y_1 - \frac{y_1^3}{6} + \frac{y_1^5}{40} - \cdots\right] \tag{7}$$

where $y_1 = y(t_1)$ and N is the number of samples. To allow the higher-order terms to contribute less than 1 deg of phase noise error, the condition

$$y_1 \leqslant 0.32$$

must be met, and to allow a maximum amplitude error of ±0.3 dB, the condition

$$y_1 \leqslant 0.64$$

must be met. This constrains the upper-limit SNR (and dynamic range) for sensibly linear operation of the 1-bit correlator.

For simplicity, one may summarize that for accurate amplitude measurements with the 1-bit correlator using CW or Gaussian noise sources, the condition

$$T_{ai} \leqslant 0.5\, T_{si}$$

must be met. In the CW case, this is also the upper-limit condition for accurate phase measurements. (In principle, oversampling could solve this problem. However, since the CW signal is not compatible with the 1-bit correlator architecture, this application is not elaborated upon.)

The best possible performance available from a 1-bit digital correlator can now be analyzed.

1. Case I. One of the strongest usable natural radio sources at X-band is 3C84, with a flux density of 46.6 Jy.[3] For a short baseline, such as between a 70-m and 34-m antenna at the same complex, it is unresolved.

Assuming 65 percent efficiency for both 70-m and 34-m antennas, $T_{a1} = 42.21$ K for the 70-m antenna and $T_{a2} = 9.95$ K for the 34-m antenna with $T_{s1} = T_{s2} = 30$ K. T_{a1} does not satisfy the linearity condition, but since it is only about 4.6 dB away, one may ignore it for a moment, assuming a simple solution can be provided. The MKIIIA 1-bit real-time correlator, designed at the Haystack Observatory, has a channel bandwidth of 2 MHz, and JPL is planning to integrate 10 channels in July 1989.

[3] Jy = 10^{-26} W/m^2 Hz.

Assuming an integration time of 0.1 sec and 1 channel, the beam-peak SNR can be calculated using Eq. (3):

$$SNR_{max} = 0.43\sqrt{\left[\frac{(42.21)(9.95)}{(72.21)(39.95)}\right][(4)(10^6)(0.1)]}$$

$$= 103.77$$

This is an SNR of 40.3 dB.

To calculate the dynamic range, take $SNR = 1$ as a reference minimum, then

$$SNR_{min} = 1$$

$$= 0.43\sqrt{\left[\frac{(T_{a1_{min}})(9.95)}{(72.21)(39.95)}\right][(2)(2)(10^6)(0.1)]} \tag{8}$$

$$T_{a1_{min}} = 0.0039 \text{ K}$$

and the dynamic range

$$DR = \frac{T_{a1_{max}}}{T_{a1_{min}}} = \frac{42.21}{0.0039} = 10823 \text{ or } 40.3 \text{ dB}$$

Assuming all ten channels[4] can be utilized in a real-time measurement configuration

$$SNR_{max} = 51 \text{ dB}$$

It has already been shown [3] that a Move-Stop-Integrate approach to DSN holography is totally unacceptable. However, assuming that the antenna can be moved slowly enough (as long as it is stable) to relax the integration time requirements to perhaps 0.5 sec (only acceptable for low-resolution scans),

$$SNR_{max} = 58 \text{ dB}$$

[4] In the current operational architecture of the Haystack correlator and its interfacing computer, the minimum integration period that can be achieved with multi-channels is 0.5 sec. No changes to the Haystack design are planned at JPL. The above analysis assumes a new computer design, and interfaces to the correlator to achieve the required 0.1-sec integration period capability would be provided (private communication, Charles Edwards).

It is anticipated that for the year 1992, a 1-bit correlator with a bandwidth of 16 MHz will be operational at JPL.[5] With this in place, a 50-dB SNR_{max} could be obtained with a 0.1-sec integration period.

2. Case I: Summary. As can be seen, the integration period and the bandwidth in the correlator are the critical parameters for obtaining high SNR and dynamic range, and are the limiting factors (assuming all the bandwidth needed is available from the radio star). Using a 1-bit correlator to obtain low-resolution holographic images is feasible and valuable for the DSN in-band holographic quick "health check" measurements. An estimated array size of up to 51 X 51 providing lateral resolution of approximately 1.6 m (0.8 m) with accuracy of 0.2 mm can be delivered for the 70-m (34-m) antenna. The source would be tracked near meridian transit to minimize elevation angle changes. Two large DSN antennas would have to be allocated for the measurement.

3. Cases II and III: Strong Source Case. The most effective strong sources are obtained from geostationary satellite downlink channels. Only the portion of the channel bandwidth that is continuously occupied is useful for the correlator. In addition, wide-bandwidth signals are more favorable than narrow-bandwidth signals (even if the narrowband signal is of stronger EIRP) in terms of SNR and dynamic range in the 1-bit correlator system, since saturation and non-linearity occur if T_a exceeds the level specified above. For now, the CW case shall be ignored and instead the alternative wideband downlink signals will be considered. Some communication satellite telephone and data links have the characteristics of Gaussian random noise. In terms of the correlator performance, they can be treated as extremely strong natural radio point sources of limited bandwidth.

About one quarter of all communication satellites have wide-bandwidth data-link signal characteristics that are useful for holographic measurements. Data links that do not occupy the channel bandwidth continuously are of no use, and those that fluctuate in intensity are serious sources of error in the correlator measurement system. Since the correlator multiplies the two channels, any amplitude variation in the signal level will not be canceled, and will cause an error in the holographic maps. This characteristic alone is considered a major drawback. Unlike the natural radio sources of large bandwidth, the satellite channel bandwidth is limited, and most of the time only a portion of the spectrum has adequate characteristics; 0.5 MHz is conservatively chosen.[6] Theoretically, one could rent a transponder on a satellite, thereby enabling an adequate wide-bandwidth noise source. This approach is considered to be impractical. Typically, the satellite signals will produce a T_a on both test and reference antennas greater than 40 dB (70-m antenna) and 34 dB (34-m antenna) above T_s.

For example, assume that when the test antenna (70-m) is observing the signal on beam peak, $T_a(\text{dB}) - T_s(\text{dB}) = 40$ dB, which is a practical consideration. Under this condition, only when the test antenna scans −43 dB below the beam peak (as shown earlier), does the correlator enter into its linear region. Taking a 0.1-sec integration period:

$$SNR_{max} = (0.43)(0.33)\sqrt{(2)(0.5)(10^6)(0.1)}$$

$$SNR_{max} = 33 \text{ dB}$$

assuming a Ku-band measurement and $T_{si} = 200$ K.

From the simple analysis above, it is seen that for strong satellite signal sources, when $T_a \gg T_s$ (hence, the reference antenna channel is saturated), the SNR and dynamic range of the 1-bit correlator are functions of the bandwidth (which is limited by the satellite) and the integration time. Since the SNR is independent of the size of the antennas, a small reference antenna should be used (D ~ 2 m) for economy. One way of overcoming the limited dynamic range of the correlator is to use a radiometer in conjunction with the correlator. Under this split architecture, the radiometer is used to measure amplitudes at signal levels above which the correlator is saturated, and the correlator provides phase information. As the antenna measurement proceeds down to its sidelobes, the radiometer is reaching its noise floor, and the correlator enters into its linear region, providing amplitude and phase measurement capability (Fig. 1).

4. Cases II and III: Summary. Even with strong satellite signal sources, the 1-bit correlator by itself has a limited dynamic range for its linear region as a phase/amplitude measurement system. The limited satellite bandwidth and short integration period required limit the correlator's linear dynamic range to about 33 dB (which is less than what can be achieved with radio stars of wide bandwidth, i.e., 50 dB).

With Gaussian noise-like signals, the correlator can provide accurate phase measurement, even in its non-linear region, and with the addition of another instrument (e.g., a radiometer), an overall large dynamic range can be achieved equal to the sum of the correlator dynamic range plus ($T_{a_{max}}$(dB) − T_s (dB)). Unavoidable signal level fluctuations and the fact that the correlator is a channel multiplication device could produce serious sources of error in the holographic map than cannot be

[5] Dave Rogstad, private communication.

[6] B. Corey (Haystack Observatory) and W. Johnson (Multicomm, Inc., Arlington, Virginia), private communication.

recovered without additional instrumentation. Using two separate instruments to measure a complex quantity, one device measuring amplitude while the other provides phase, is an undesirable approach. Using two separate instruments in an overlapping fashion (as one saturates on its upper SNR the other reaches its lower limit) is clearly not a recommended instrumentation approach. There are other feasible ways to extend the dynamic range of the 1-bit correlator. For example, switched attenuators may be incorporated to drive the correlator into its linear range at strong signal levels. The attenuators can then be switched out at the lower signal level, maintaining the correlator in its linear range. None of these techniques, however, can take advantage of stronger satellite signal sources and provide a larger SNR at the correlator output. All they do is extend the dynamic range of the 1-bit correlator. This is the result of a fundamental mismatch between strong signals and the 1-bit correlator architecture. In view of the above, and since better system solutions are available, additional analysis for Cases II and III is unnecessary.

Some radio astronomy observatories perform limited holographic measurements using the above approach because of the availability of the instruments already connected to their system. (See summary in Table 1.)

B. Narrow-Bandwidth System

The narrow-bandwidth system can be designed with a wide dynamic range and linear response. A narrow-bandwidth receiver/data acquisition system design and recommendation for JPL holography implementation was formally proposed in October 1985.[7] The system makes use of geostationary satellite beacon signals (nearly CW) available on nearly all satellites at Ku-band (11.45 GHz), X-band (7.7 GHz), S-band (2.2 GHz) and perhaps on other bands in the future. The IF section of the new HP 8510B network analyzer phase locked with an HP 8530B sweep oscillator could provide the heart of this system architecture (Fig. 2). Rather than cross-correlating the two channels, which is a multiplicative operation, the HP 8510B uses synchronous detectors for the I and Q components of the test and reference channels. After digitization (19-bit resolution A/D converter), the ratio of test-to-reference channel is formed to provide the real and imaginary components of the complex far-field function. Amplitude variations in the satellite signal cancel out in the division operation. This feature is especially critical since no control over the satellite signal power level is reasonable. Also, since the reference channel SNR in this scheme can easily be 40 dB or better, it can be safely used in the denominator (this would not be desirable for weak reference signals). Doppler frequency changes and phase jitters due to satellite signal instabilities will produce a frequency difference between the second local oscillator (LO) and IF signals (Fig. 2) that will be measured by the HP 8510B, which then generates an error signal that phase locks the LO to produce the 20-MHz second IF input to the HP 8510B.

The HP 8510B provides a linear dynamic range of better than 96 dB down to integration periods of 0.2 msec (which covers the future high-resolution, high-speed 70-m/4-hr goal). With a satellite beacon EIRP of about 11 dBW, a beam-peak SNR of 73 dB can be achieved on the 70-m antenna with a 0.1-sec integration period and a simple room-temperature FET amplifier, while a 2.8-m reference dish can provide more than 44 dB in SNR using a room-temperature FET.

For the HP 8510B architecture, it can be shown that the effective signal SNR is

$$SNR_E = \frac{1}{\sqrt{\frac{1}{SNR_T^2} + \frac{1}{SNR_R^2} + \frac{1}{SNR_T^2\, SNR_R^2}}} \tag{9}$$

where SNR_T and SNR_R are the test channel SNR and reference channel SNR, respectively. This expression is also correct for a multiplier integrator as well as a divider integrator.

From Eq. (9), it is apparent that the effective SNR_E is dominated by the weaker of the two channels. What this means is that the beam-peak SNR of 73 dB is not realized, and the first few data points on beam peak and a few sidelobes have an effective SNR of 44 dB (the reference SNR). Once the test channel SNR drops below 44 dB, the reference antenna does not hurt the effective SNR_E, which, from that point, follows the same function as the test antenna beam patterns (SNR_T). Also, since very few data points are affected (approximately 0.5 percent), and since by the nature of the data processing through the Fourier Transform operation all the data points in the far-field contribute to each and every point in the aperture, this is acceptable, as shown below.

To evaluate the suitability of the HP 8510B architecture with a small reference antenna, a simulation algorithm was written in which each channel of the I and Q components of both the test and reference channels had added independent noise processing components n, for which the one sigma (1σ) in the random Gaussian function are

$$1\sigma_T = \frac{Amp_T(\theta_{max})}{SNR_T(\theta_{max})} \tag{10}$$

[7] D. J. Rochblatt, "JPL Holography Review" (internal document), October 10, 1985.

and

$$1\sigma_R = \frac{Amp_R}{SNR_R} \tag{11}$$

for the test and reference signals, respectively. The function of the IF section of the HP 8510B was simulated to provide the resultant measured complex quantity including noise:

$$\text{Measured Complex Field} = \frac{Amp_T(\theta_i)\, e^{j\phi_{Ti}} + n_{R_i}^T + jn_{I_i}^T}{Amp_R\, e^{j0} + n_{R_i}^R + jn_{I_i}^R} \tag{12}$$

where the real and imaginary components of the noise processing are denoted by subscripts R_i and I_i, respectively. During this simulation, the effect of the SNR of the reference and test antennas on measurement accuracy was examined.

In the simulation, four rings of panels were intentionally displaced by 0.2 mm (λ/130 at 11.45 GHz). Three rings were displaced positively and one was displaced negatively. The width of the three outermost rings is 2.0 m (76λ) and the innermost ring is 1.0 m wide. The rms surface error of this model is 0.11 mm. The far field for the above reflector geometry was generated [7] and then contaminated with noise, due to the front end, according to the Eq. (12) model. The far-field data were then processed by the JPL DSN holography software [8] to display the recovered surface error maps and compute the surface rms errors.

In Simulation I (Figs. 3 and 4), the far field was processed with no noise added to it. This simulated an SNR of more than 90 dB. The computer computational errors are at a level of about λ/5000 (11.45 GHz). By subtracting the Simulation I model from subsequent simulations (map differencing), a measure comparable to measurement system standard deviation is obtained.

Simulation II (Figs. 5, 6, and 7; note the different scales in the cut plot between Simulation I and all subsequent simulations), models the conditions where the test antenna SNR on beam peak in a 0.1-sec integration period is 78 dB and the reference antenna constant SNR is 40 dB. These conditions are stated as a goal but are not usually achieved in practice. The recovered rms of the test antenna surface is 0.11 mm and the measurement system standard deviation is 0.04 mm (λ/650 at 11.45 GHz).

Simulation III (Figs. 8, 9, and 10) simulates the presently achievable condition in which the test antenna beam peak SNR in a 0.1-sec integration period is 73 dB and the reference antenna SNR is 40 dB. The recovered surface rms is 0.12 mm with a standard deviation of 0.07 mm (λ/370 at 11.45 GHz). In the cut plot, Fig. 9 in this case, the aperture amplitude taper of −13 dB was superimposed for demonstration of increased error in the image toward the edge of the dish. Simulations IV, V, and VI (Figs. 11 through 19) and Table 2 demonstrate the conditions of decreasing SNR in the test channel and increasing SNR in the reference channel in 5-dB steps. The necessity of high beam-peak SNR for high-resolution, high-precision holographic measurement is clearly demonstrated. Also, the limited contribution of reference channel SNR in compensation for low test-channel SNR is demonstrated and shown. The limited contribution of the reference channel SNR-to-surface error reconstruction relates to the relatively small number of data points being affected (0.5 percent for the case 73 dB/40 dB), and to the physics, i.e., the small surface distortions (high frequency) affect mostly the sidelobes farther away from the beam peak [3]. Thus, one of the more important functions of the reference SNR in the CW case is to keep the receiver in phase lock with the carrier.

IV. Phase Retrieval Holography

The phase retrieval holography retrieves phase information from a measurement of the antenna far-field intensity only. Since phase is not directly measured, a second reference antenna and a two-channel receiver or correlator are not necessary. The in-place receiver and front end are used to measure the antenna far-field intensity function. For more details about the technique, see Appendices A and B.

Because of the limitations of this technique, it is only recommended for low-resolution holographic imaging sufficient for operation and maintenance quick "health check" needs. For such application, it is estimated that a beam-peak SNR of 60 dB is required in order to achieve the same precision over a 25 X 25 size array as would be achieved with true holographic (amplitude and phase) measurements. If radio star sources and a radiometer measurement system are used, a square root reduction in SNR is suffered (due to incoherent processing) relative to coherent processing using a two-channel correlator. Satellite CW beacon signals are available at S-band (2.2 GHz) from DSCS satellites, viewable at all DSN complexes with high achievable SNR and are therefore recommended for this approach.

V. Summary and Conclusion

Based on the far-field signal sources available, a narrow-bandwidth measurement system is superior in performance to a broad-bandwidth system based on a 1-bit real time correla-

tor (20-MHz BW) for high-resolution/high-precision panel setting holography. A multi-bit correlator is a better candidate for holographic measurement[8] because it provides wider dynamic ranges. In the cases where the correlator is of multi-bits, or when a synthesis signal is correlated against the 1-bit correlator, phase locking becomes necessary and essentially one comes back to an HP 8510B type of architecture.

The 1-bit correlator (Haystack, MKIIIA), expected at JPL in about one year (although implementation at all DSN complexes is not envisioned before 1994), would be useful for low-resolution holographic measurement in the DSN frequency band using natural radio sources. It has the advantage that no feeding/receiver changes need to be made for the measurement, allowing quick response to a demand for an antenna "health check." However, a second large antenna (34-m or 70-m) would have to be allocated for such measurements.

Phase retrieval holography is especially attractive for quick "health check" antenna diagnostics. Only one antenna (the antenna under test) is used, utilizing existing station receivers and front end within S-band. It is a minimal cost solution that could prove powerful for low-resolution holography.

[8] D. J. Rochblatt, "Digital-Multibit-Correlator/Remarks," JPL IOM 3331-84-053 (internal document), July 20, 1984.

For high-resolution, high-precision panel setting holography and future growth potential, the narrow-bandwidth/CW system provides significant advantages, and hence it is recommended here. In addition, this system will also perform low-resolution "health check" measurements in a shorter time with higher precision (see Table 1), albeit not in the DSN frequency bands. With some design modifications, the DSN advanced receiver could be utilized to advantage in the future.

Most of the software (80 percent) that is required for data acquisition and correction is independent of the hardware (it will apply for the narrow-bandwidth as well as the 1-bit correlator system). Also, all the JPL DSN holography data processing and the holography software methodology developed in-house thus far are independent of the system hardware.

It is strongly recommended that the DSN initiate holography capability with a narrow-bandwidth system capable of both high- and low-resolution holography measurements. An HP 8510B or other commercial instrument (with manufacturer's support for perhaps 10 years) is recommended as the heart of the narrow-bandwidth high/low-resolution implementation. With modest software addition, the wide-bandwidth 1-bit correlator could become part of that system, providing low-resolution maps in the DSN frequency band. Phase retrieval holography is especially attractive for satisfying the requirement for a quick response to DSN Operations' needs.

Acknowledgments

The author wishes to thank Brooks Thomas of the Tracking Systems and Applications Section for his many helpful technical discussions and contributions. In addition, thanks are due to D. Bathker and B. Seidel for brainstorming discussions, and to V. Galindo for his contributions to the minimization technique described in Appendix B.

References

[1] P. F. Scott and M. Ryle, "A Rapid Method for Measuring the Figure of a Radio Telescope Reflector," *Mon. Not. Roy. Astr. Soc.*, vol. 178, pp. 539–545, 1977.

[2] L. R. D'Addario, "Holographic Antenna Measurements," *Memo No. 202*, National Radio Astronomy Observatory, Charlottesville, Virginia, pp. 1–20, November 1982.

[3] D. J. Rochblatt and B. L. Seidel, "DSN Microwave Antenna Holography," *TDA Progress Report 42-76*, vol. October–December 1983, Jet Propulsion Laboratory, Pasadena, California, pp. 27–42, February 15, 1984.

[4] A. R. Thompson, J. M. Moran, and G. W. Swenson, Jr., *Interferometry and Synthesis in Radio Astronomy*, New York: John Wiley & Sons, Inc., pp. 155–168, pp. 247–305, 1986.

[5] J. H. Vleck and D. Middleton, "The Spectrum of Clipped Noise," *Proceedings of the IEEE*, vol. 54, no. 1, pp. 1–56, January 1966.

[6] J. B. Thomas, "An Analysis of Long Baseline Radio Interferometry, Part II," *JPL Technical Report 32-1526*, vol. VIII, 1972.

[7] Y. Rahmat-Samii and D. J. Rochblatt, "Effect of Measurement Errors on Reflector Surface Reconstruction Using Microwave Holographic Metrology," *Proceedings of the Antenna Measurement Techniques Association*, Seattle, Washington, pp. 174–179, Sept. 1987.

[8] D. J. Rochblatt, Y. Rahmat-Samii, and J. H. Mumford, "DSN Microwave Antenna Holography Part II: Data Processing and Display of High Resolution Effective Maps," *TDA Progress Report 42-87*, vol. July–September 1986, Jet Propulsion Laboratory, Pasadena, California, pp. 92–97, 1986.

[9] R. E. Burge, "The Phase Problem," *Proc. R. Soc. Lond. A.*, vol. 350, pp. 191–212, 1976.

[10] A Walter, "The Question of Phase Retrieval in Optics," *Opt. Acta*, vol. 10, pp. 41–49, 1963.

[11] R. W. Gerchberg and W. O. Saxton, "A Practical Algorithm for the Determination of Phase from Image and Diffraction Plane Pictures," *Optik*, vol. 35, pp. 237–246, 1972.

[12] D. L. Misell, "A Method for the Solution of the Phase Problem in Electron Microscopy," *J. Phys. D., Appl. Phys.*, vol. 6, pp. L-6–L-9, 1973.

Table 1. System performance (70-m antenna)

System type	Bandwidth, MHz	Signal source	Frequency, GHz	D_R, m	T, sec	SNR_{max}, dB	DR, dB	Array size, n × n	δ, m	σ, mm	Measurement time, hr
A	2	3C84	8.4	34	0.1	40.3	40.3	25 × 25	3.3	0.80	0.5
A	20	3C84	8.4	34	0.1	51	51	25 × 25	3.3	0.24	0.5
A	20	3C84	8.4	34	0.5	58	58	51 × 51	1.6	0.22	4.0
A[a]	0.5	Satellite	11.45	34/2.8	0.1	33	73	127 × 127	0.65	0.3	6.0
B	0.01	Satellite Beacon	11.45	2.8	0.1	73	96	197 × 197	0.40	0.1	12.0
B[b]	0.01	Satellite Beacon	11.45	2.8	0.02	73	96	197 × 197	0.40	0.1	4.0
B	0.01	Satellite Beacon	11.45	2.8	0.1	73	96	127 × 127	0.65	0.06	6.0
B	0.01	Satellite Beacon	11.45	2.8	0.1	73	96	25 × 25	3.3	0.012	0.5
B[b]	0.01	Satellite Beacon	11.45	2.8	0.02	73	96	25 × 25	3.3	0.012	0.25
C	TBD	Satellite Beacon	2.2	Not Needed	0.1	73	73	32 × 32	3.3	0.2	0.25

A = Wide-bandwidth system
B = Narrow-bandwidth system
C = Phase retrieval
D_R = Reference antenna diameter
T = Integration period
DR = Dynamic range
δ = Lateral resolution
σ = Standard deviation of surface profiles

[a]With added radiometer for amplitude measurements and assuming $T_{a_{max}}/T_s = 4$ dB.

[b]Possible future capability.

Table 2. Narrow-bandwidth system simulations (64-m/2.8-m antennas)

Simulation No.	$SNR_{T_{max}}$, dB	SNR_R, dB	Recovered surface rms, mm	Measurement system standard deviation, mm	Figures
I	>90	n/a	0.11	0.005	3, 4
II	78	40	0.11	0.04	5, 6, 7
III	73	40	0.12	0.07	8, 9, 10
IV	68	45	0.16	0.13	11, 12, 13
V	63	50	0.25	0.23	14, 15, 16
VI	58	55	0.43	0.41	17, 18, 19

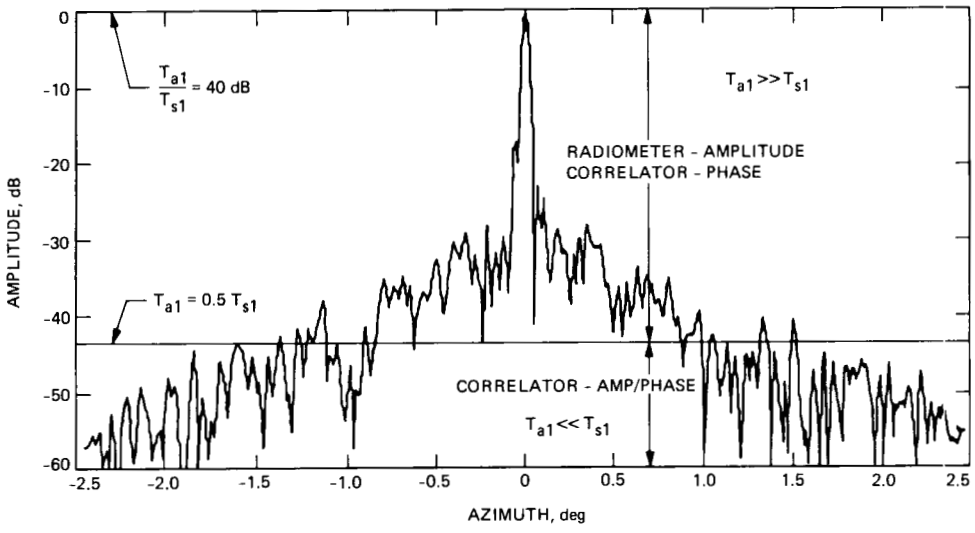

Fig. 1. Conceptual measurement scheme utilizing broadband satellite channels and radiometer/correlator in an overlapping, saturation mode.

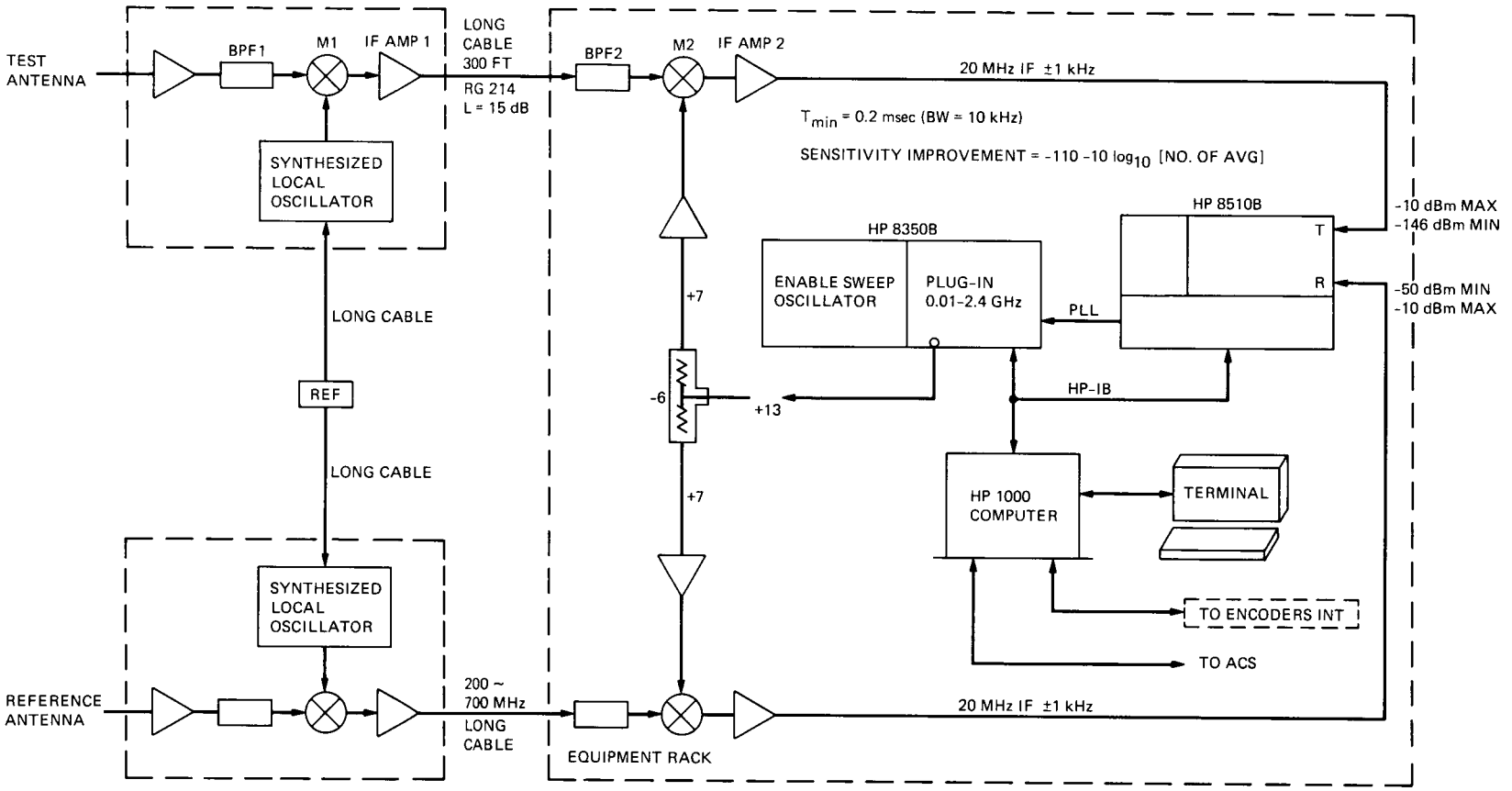

Fig. 2. Block diagram of narrow-bandwidth holographic measurement system.

ORIGINAL PAGE
COLOR PHOTOGRAPH

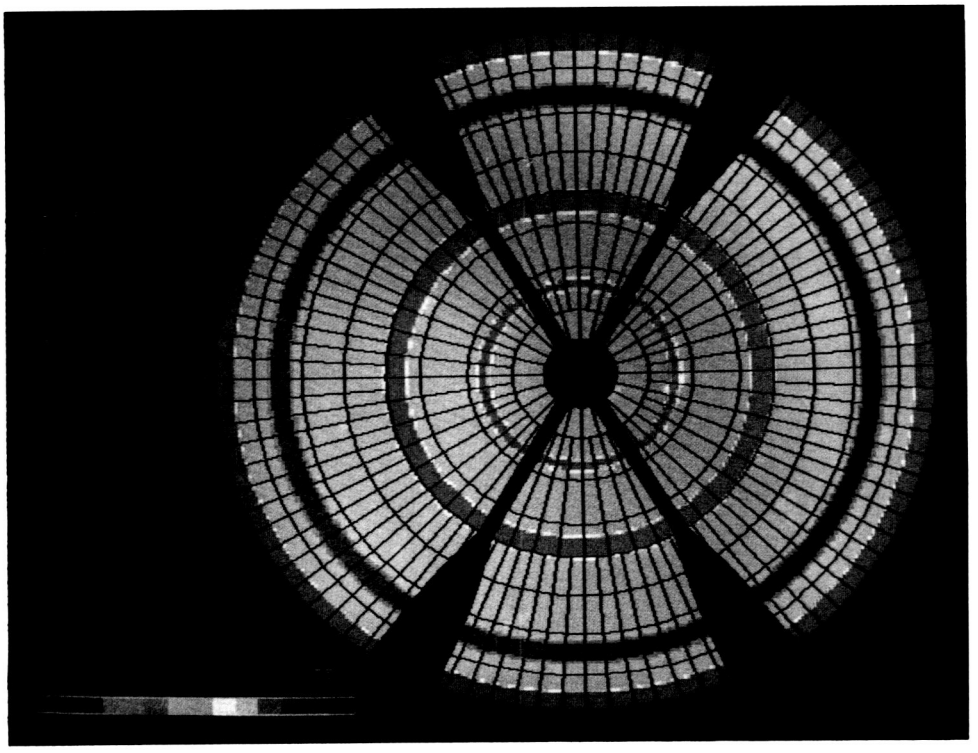

Fig. 3. Surface error map for the parameters in Table 2, No. I.

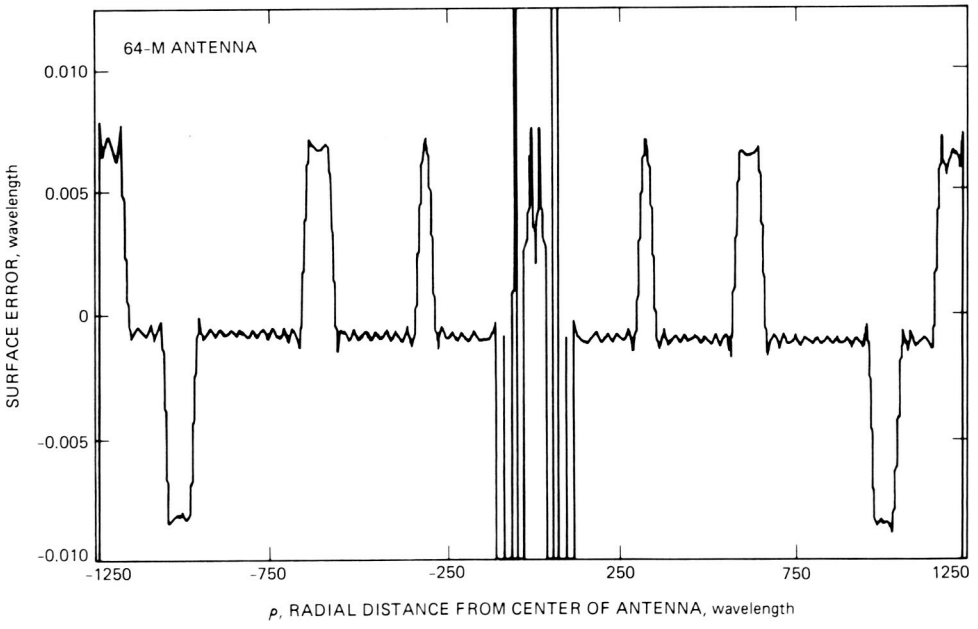

Fig. 4. Cut plot of No. I.

ORIGINAL PAGE
COLOR PHOTOGRAPH

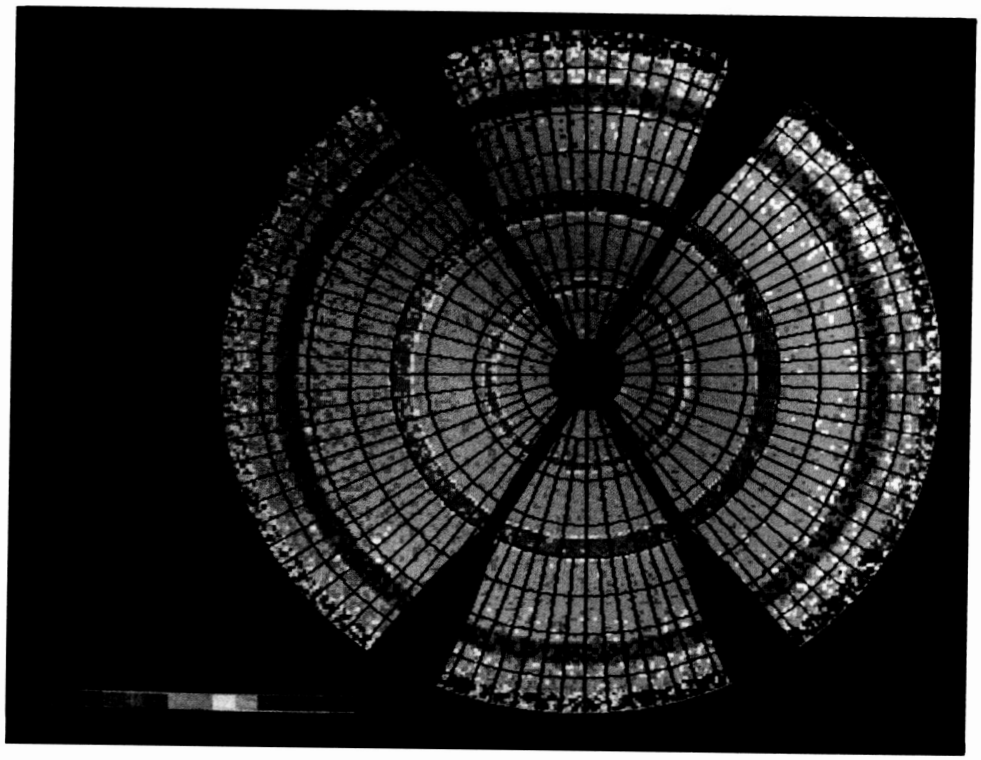

Fig. 5. Surface error map for the parameters in Table 2, No. II.

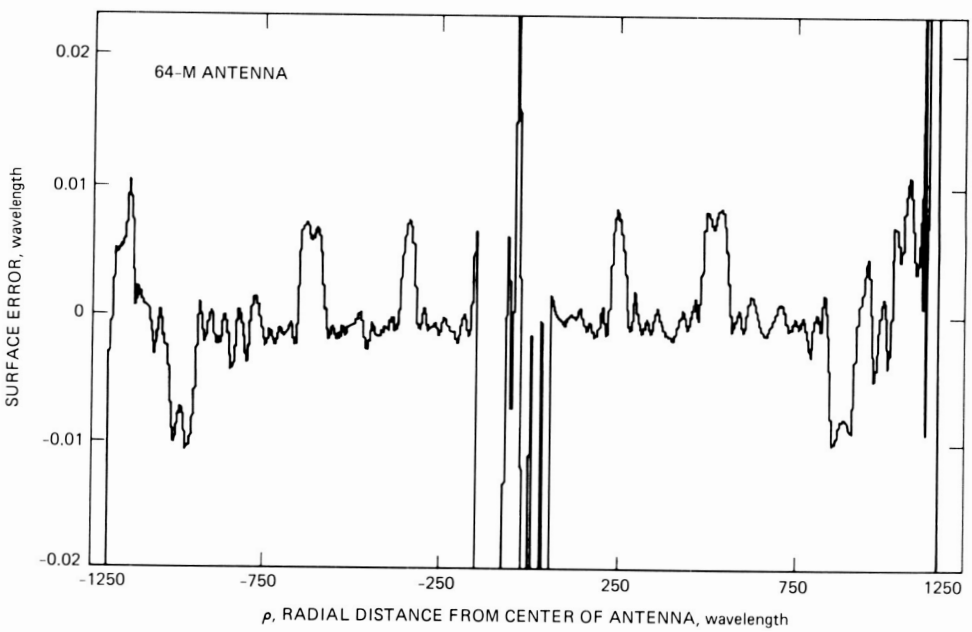

Fig. 6. Cut plot No. II.

ORIGINAL PAGE
COLOR PHOTOGRAPH

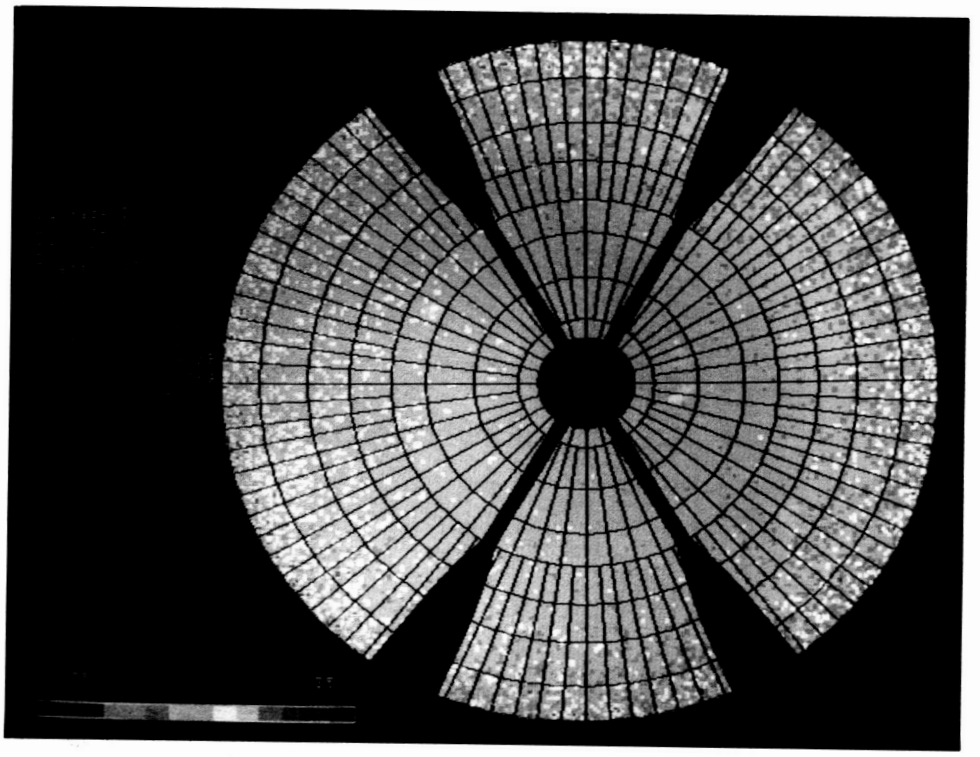

Fig. 7. Map differencing No. II.

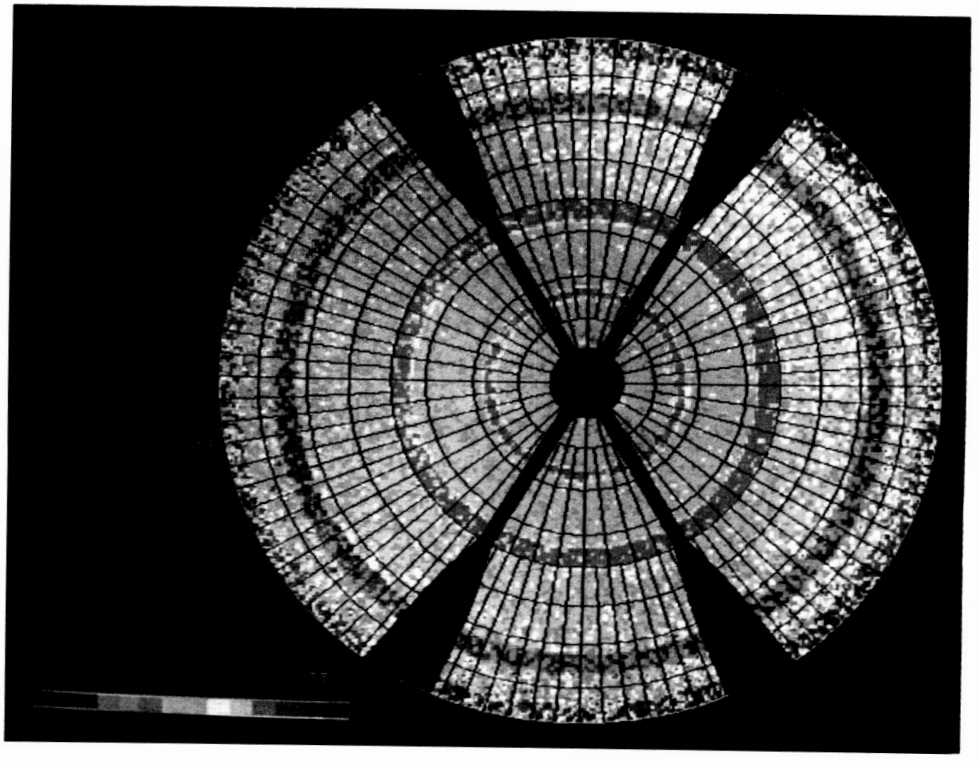

Fig. 8. Surface error map for the parameters in Table 2, No. III.

ORIGINAL PAGE
COLOR PHOTOGRAPH

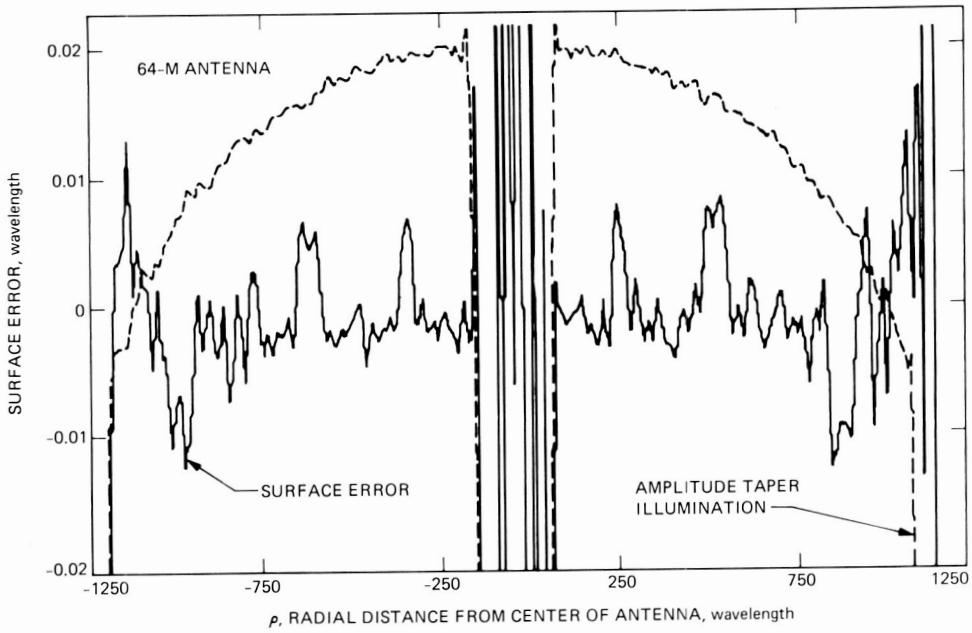

Fig. 9. Cut plot No. III.

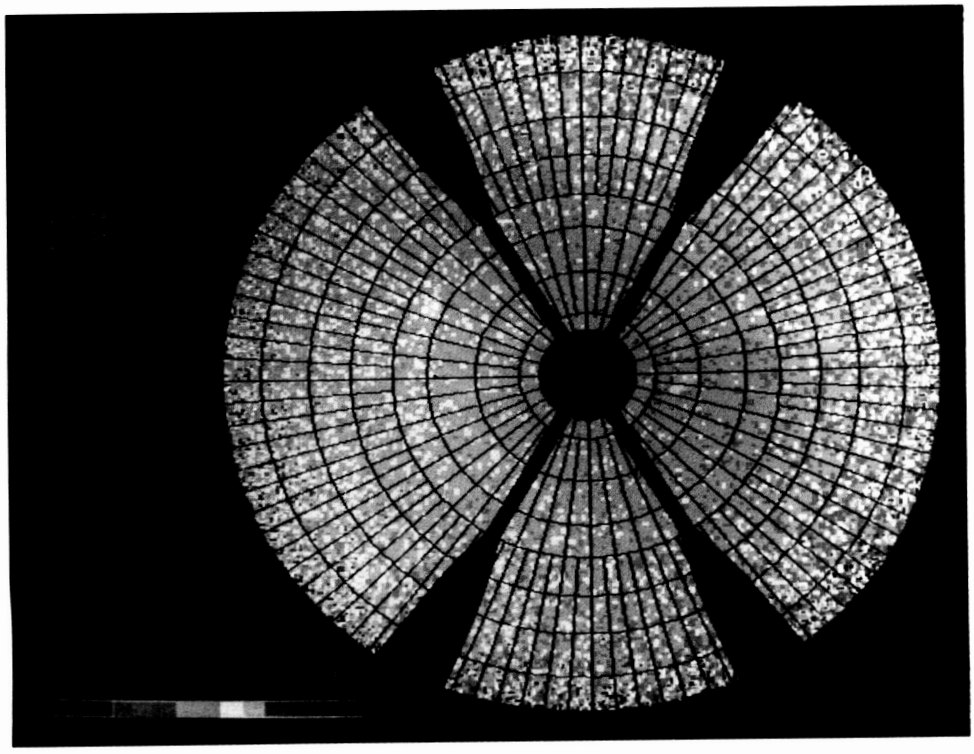

Fig. 10. Map differencing No. III.

ORIGINAL PAGE
COLOR PHOTOGRAPH

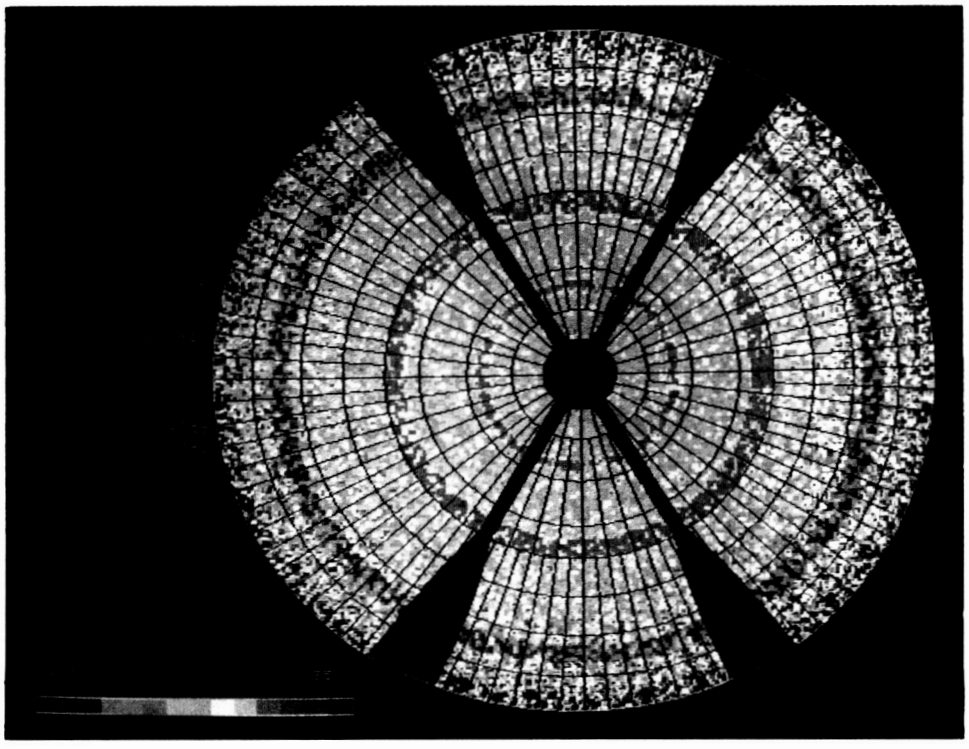

Fig. 11. Surface error map for the parameters in Table 2, No. IV.

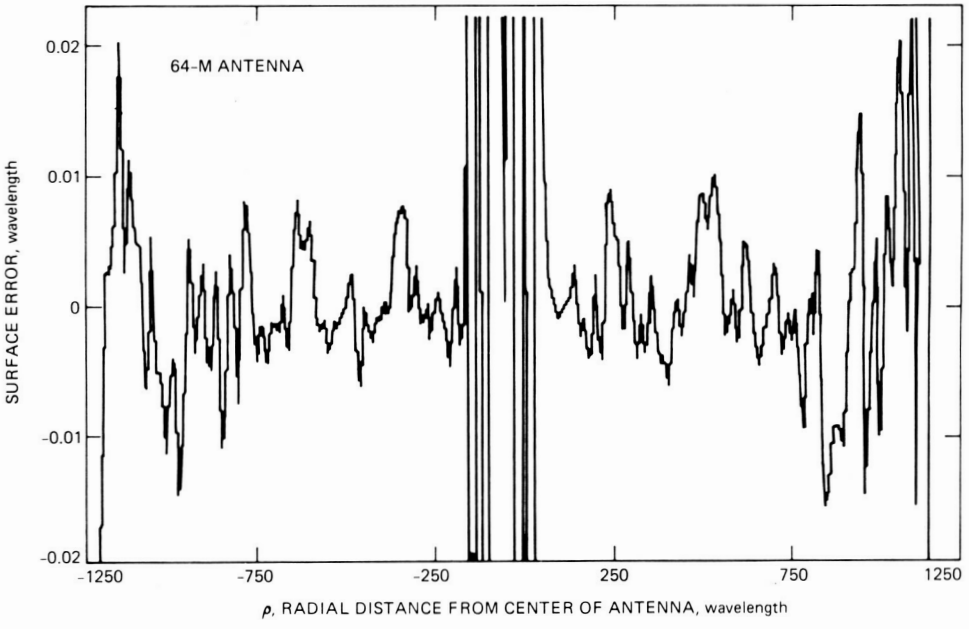

Fig. 12. Cut plot No. IV.

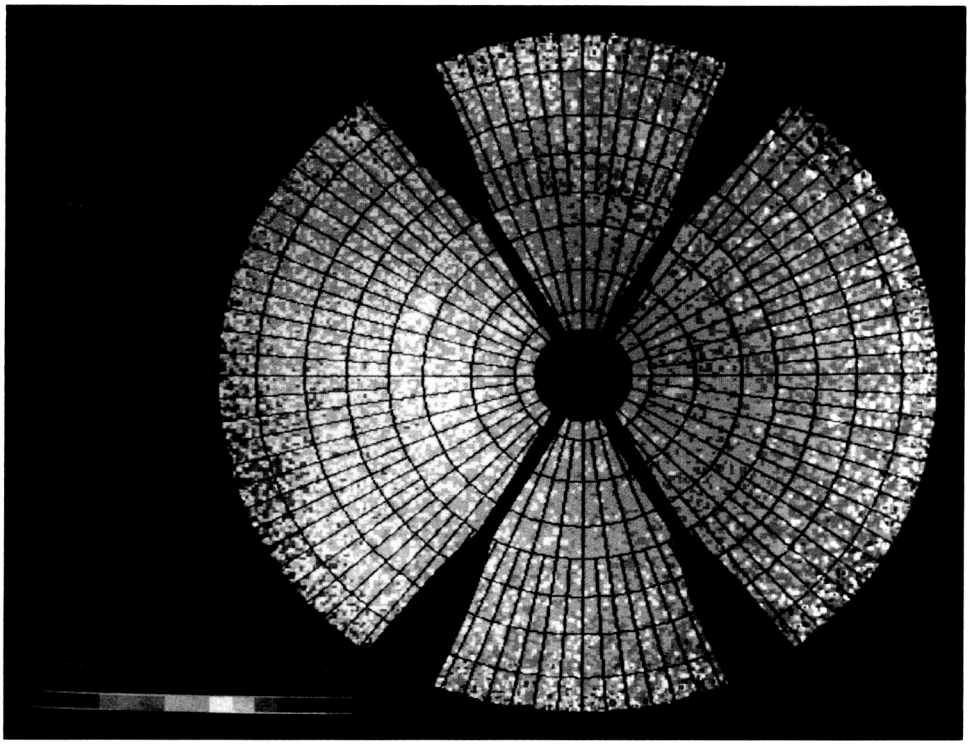

Fig. 13. Map differencing No. IV.

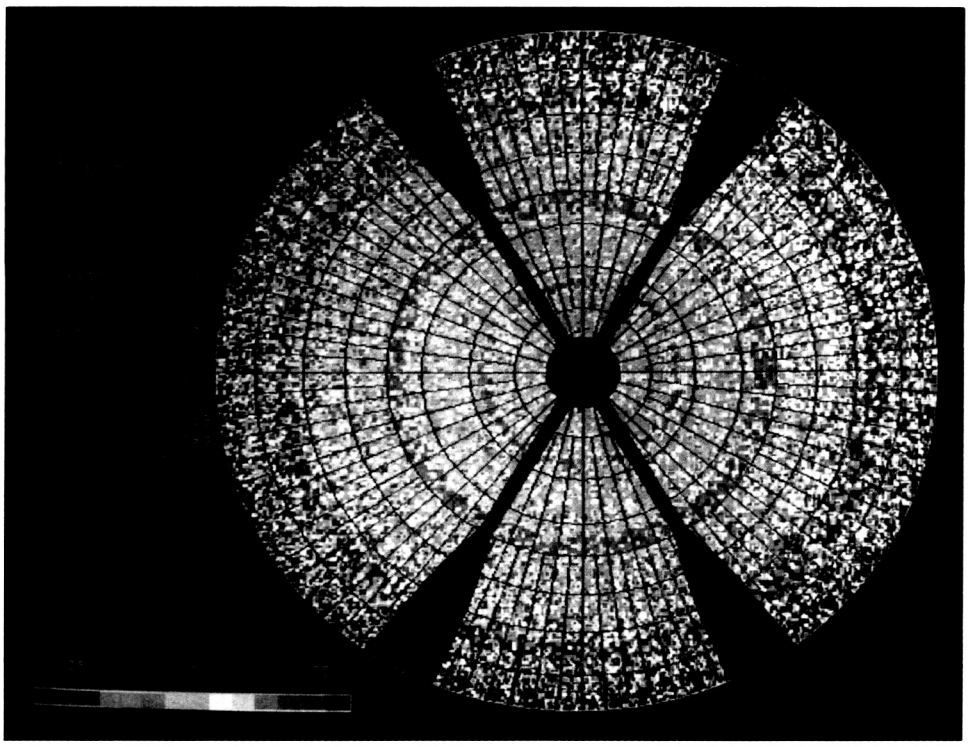

Fig. 14. Surface error map for the parameters in Table 2, No. V.

ORIGINAL PAGE
COLOR PHOTOGRAPH

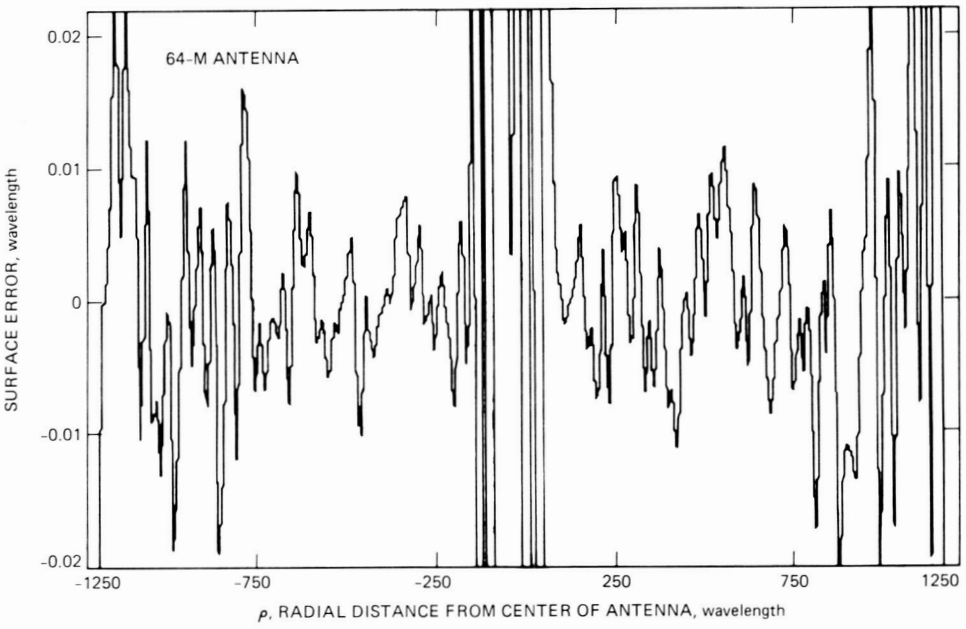

Fig. 15. Cut plot No. V.

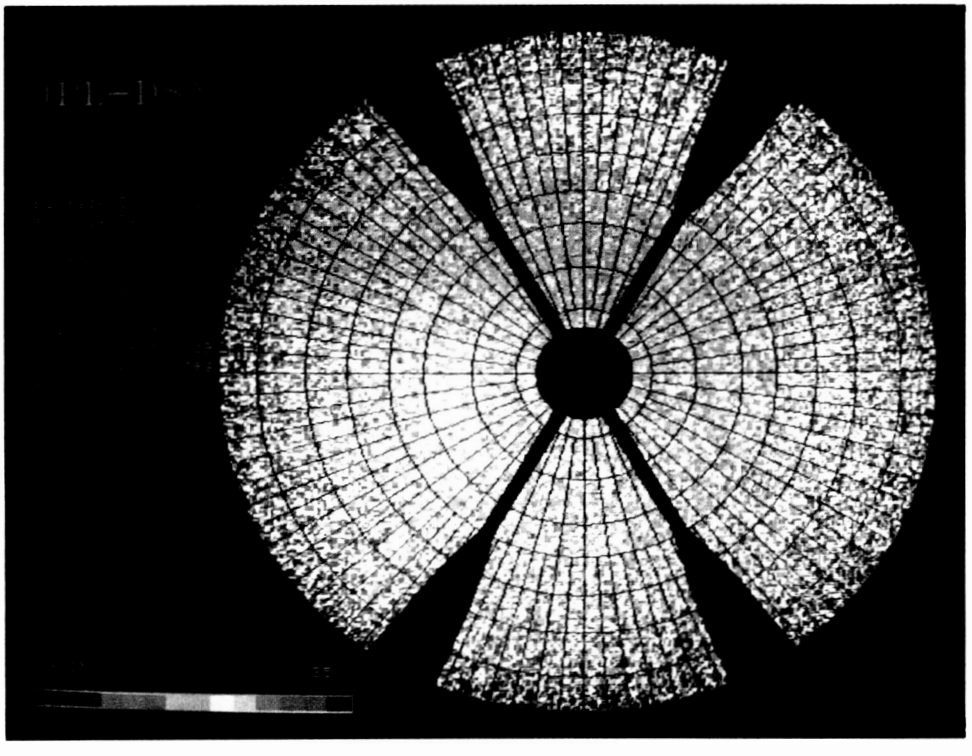

Fig. 16. Map differencing No. V.

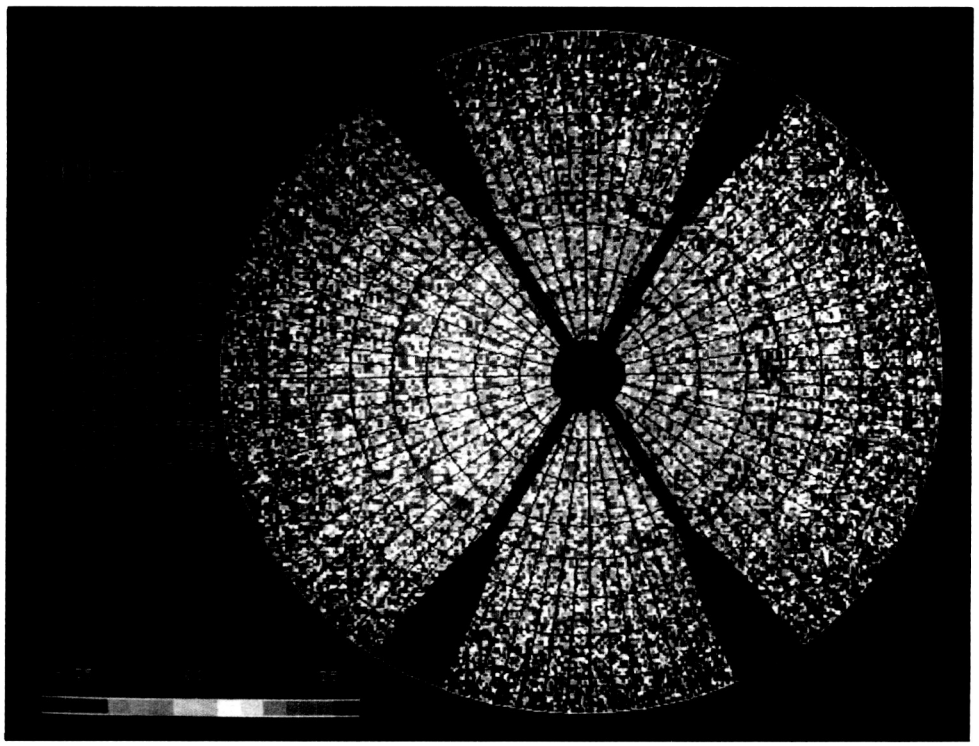

Fig. 17. Surface error map for the parameters in Table 2, No. VI.

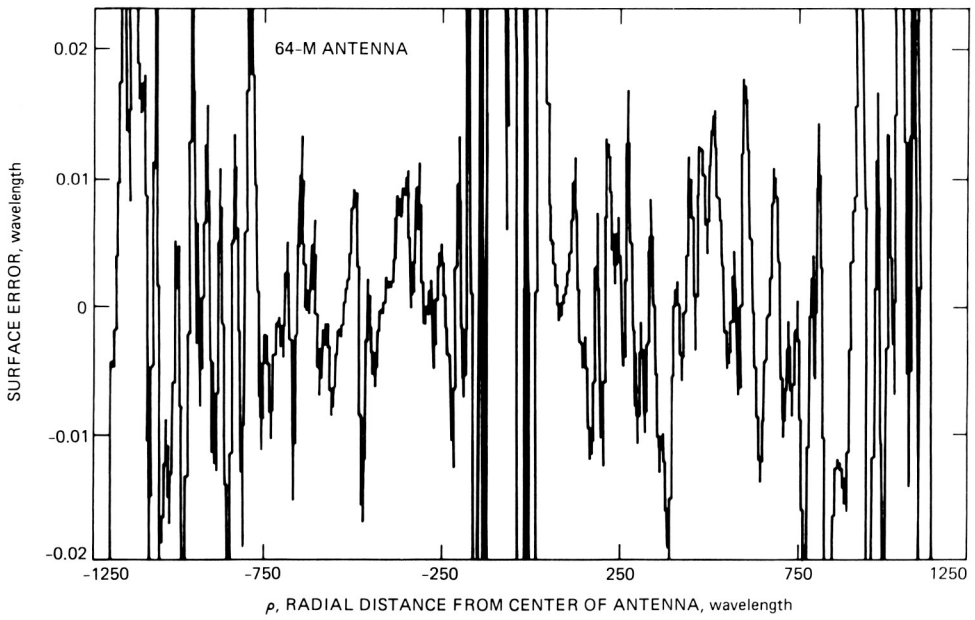

Fig. 18. Cut plot No. VI.

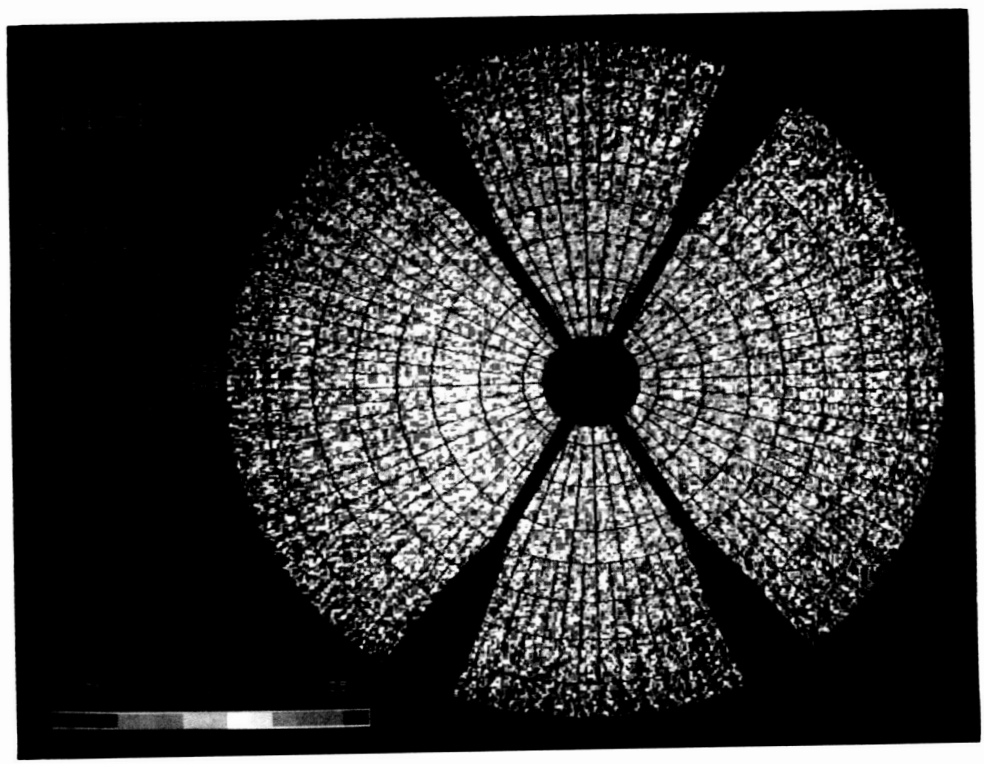

Fig. 19. Map differencing No. VI.

Appendix A

Phase Retrieval Holography Technique

The antenna aperture function $f(x)$ is band-limited to a given range (the antenna diameter).

$$f(x) = 0 \qquad x > d \tag{A-1}$$

(For simplicity of illustration, functions of one variable shall be used without loss of generality.)

For a smooth $f(x)$, the magnitude of the far-field function $F(u)$ will essentially be contained in a band U_{max}. Under these conditions. the Fast Fourier Transform (FFT) is valid and the far-field and aperture-field functions can be related by:

$$f(x) = F^{-1}\{F(u)\} \tag{A-2}$$

and

$$F(u) = F\{f(x)\} \tag{A-3}$$

where F and F^{-1} denote the FFT and IFFT operators, respectively.

For this band-limited function, the Hilbert Transform can be applied:

$$\text{Imag}\, F(u) = H\{\text{Re}\, F(u)\} \tag{A-4}$$

$$\text{Re}\, F(u) = -H\{\text{Imag}\, F(u)\} \tag{A-5}$$

where H denotes the Hilbert transform, and Re and Imag denote the real and imaginary parts of a complex function.

Numerical procedures can now be employed to obtain the phase of $F(u)$ from a knowledge of $|F(u)|^2$, the measured far-field intensity function [9]. Generally, a unique solution will not be obtained, since $F(z)$, $z = x + jy$, is an entire transcendental function and not a finite polynomial.

A transcendental entire function has infinitely many zeros where a zero z_k of $F(z)$ is a solution of

$$F(z_k) = 0 \tag{A-6}$$

which corresponds to an intensity null in the far-field function.

$F(u)$ is the projection on the real axis (of the complex plane) of the entire function $F(z)$, which is encoded by its zeros z_k. Another entire function, $F^1(z)$, which has a flipped zero z_k^* across the real axis, will have the same modules as $|F(u)|$ or

$$|F^1(u)| = |F(u)| \tag{A-7}$$

Therefore, a unique phase solution cannot be obtained without some further information that will allow the removal of phase ambiguity [10].

The additional information required to solve the phase uniqueness problem can be acquired from intensity information of the Geometrical Theory of Diffraction (GTD)-predicted aperture field functions, or previously derived aperture intensity functions from holographic measurements performed at the same measured frequency, i.e., S-band. Figure A-1 demonstrates the excellent agreement between the envelopes of the GTD-predicted aperture amplitude and the actual aperture amplitude derived via holography processing from measured holographic (amplitude and phase) far-field patterns. Reflector and subreflector small misalignments are mostly noticeable in the aperture phase function, while the aperture amplitude function is mostly unchanged. The iterative approach is presented here, while Appendix B presents a minimization in one step. This error-reduction algorithm starts by transforming the aperture complex field to the far field via FFT, replacing the amplitude part by the measured amplitude, then transforming back to the aperture field via IFFT, replacing the amplitude function and repeating the procedure until convergence to a global minimum is reached. This algorithm was suggested by Gerchberg and Saxton [11]. The good initial "guess" promises convergence to the global minimum (see Fig. A-2). This minimum is the square error of the difference between the measured far-field amplitude and the iterated one.

$$E = N^{-2} \sum_{u} [|G_k(u)| - |F(u)|]^2 \tag{A-8}$$

where

N^2 = total number of data points

$|F(u)|$ = measured far-field intensity function (see Fig. A-2)

$|G_k(u)|$ = computed far-field intensity function (see Fig. A-2)

It can be shown, by application of Parseval's theorem, that the square error E will monotonically decrease or stay constant.

Another algorithm suggested by Misell [12] makes use of two measured intensity far-field functions obtained for a focused and a defocused image (subreflector position). This algorithm has been reported to have better convergence, although it is not as attractive as the algorithm presented above. The amount of additional work needed to make a decision is not large.

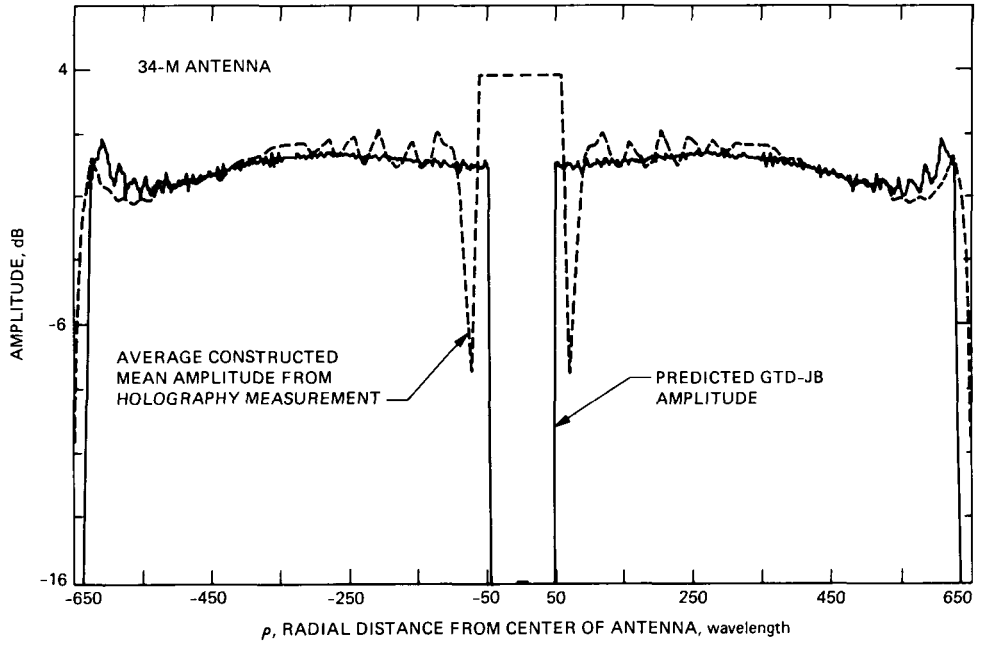

Fig. A-1. A comparison of aperture amplitude functions from GTD-predicted results (solid line) and holographic measurement data (dashed line).

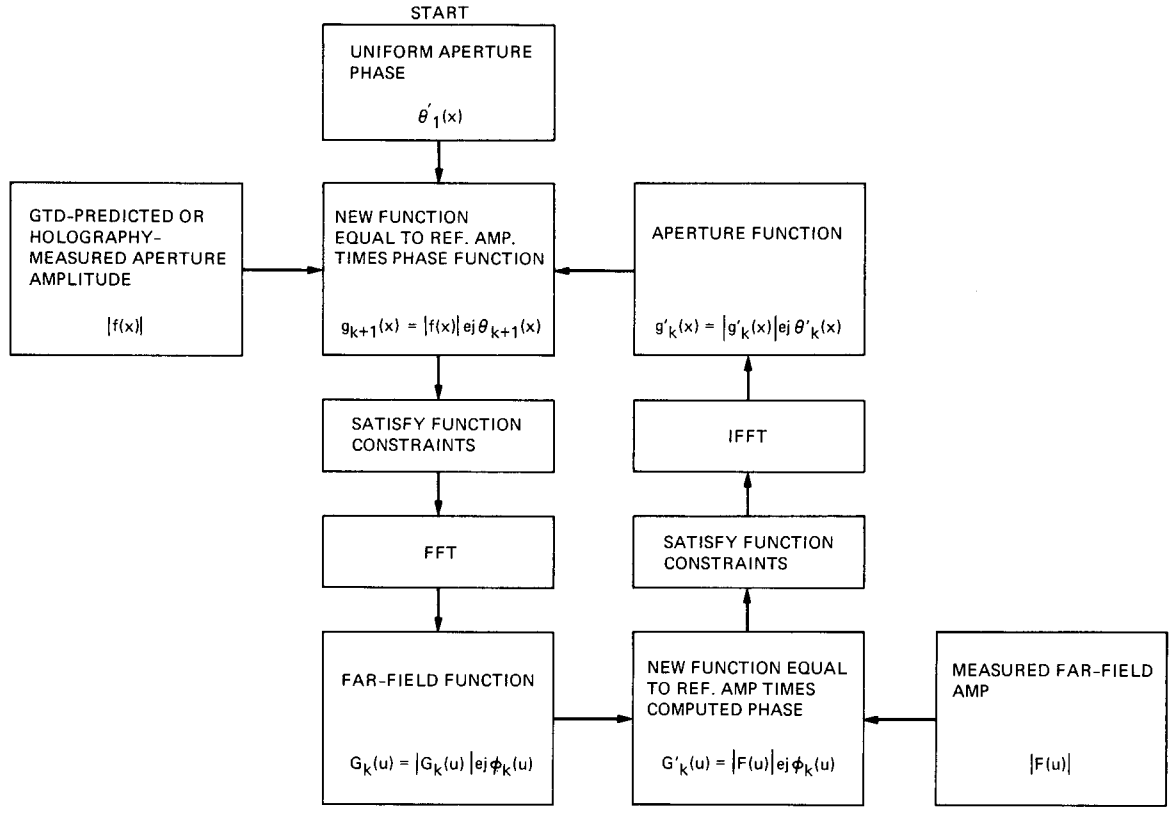

$$G_k(u) = |G_k(u)| \exp[j\phi_k(u)] = F\{g_k(x)\}$$

$$G'_k(u) = |F(u)| \exp[j\phi_k(u)]$$

$$g'_k(x) = |g'_k(x)| \exp[j\theta'_k(x)] = F^{-1}\{G'_k(u)\}$$

$$g_{k+1}(x) = |f(x)| \exp[j\theta_{k+1}(x)] = |f(x)| \exp[j\theta'_k(x)]$$

Fig. A-2. Phase retrieval (error reduction) algorithm after Gerchberg and Saxton [11].

Appendix B
Minimization Technique for Phase Retrieval Holography

The minimization technique suggested here (by Galindo and Rochblatt) will solve for the antenna aperture phase in one step, thus eliminating the iterative approach discussed in Appendix A.

This derivation assumes that the ideal antenna aperture amplitude function $A_I(x)$ is unchanged by small reflector and subreflector misalignments, and that the phase change $\delta\theta(x)$ due to those misalignments is small. These are assumptions inherent in the holographic technique in any case. The "smallness" of the aperture phase error $\delta\theta(x)$ may or may not be more stringent here.

For simplicity, all equations are derived in one dimension without loss of generality (to the two-dimension case).

Let the ideal antenna aperture function be

$$f_I(x) = A_I(x) \exp [j\theta_I(x)] \tag{B-1}$$

and the actual aperture function be

$$f(x) = A(x) \exp [(j\theta(x))] \tag{B-2}$$

The actual far-field function can now be related to the aperture function by a Fourier Transform integral:

$$F(u) = A_F(u) \exp [j\phi(u)] = \int_x A(x) \exp [j\theta(x)] \exp [-jkux] \, dx \tag{B-3}$$

Using the aperture amplitude approximation implies

$$A_I(x) \approx A(x) \tag{B-4}$$

and for the phase

$$\theta(x) = \theta_I(x) + \delta\theta(x) \tag{B-5}$$

and for small $\delta\theta(x)$

$$\exp [j\theta(x)] \approx \exp [j\theta_I(x)] \, [1 + j\delta\theta(x)] \tag{B-6}$$

It is this linearization, Eq. (B-6), of the phase error function that permits the "one step" solution for $\delta\theta(x)$.

Note that a small phase error $\delta\theta(x)$ will invariably justify the $A_I \approx A$ approximation, Eq. (B-4). Thus, the far-field function can be written

$$F(u) \approx \exp [j\theta_I] \int_x A_I(x) \, [1 + j\delta\theta(x)] \exp [-jkxu] \, dx \tag{B-7}$$

where the ideal aperture phase $\theta_I(x)$ was taken as a constant (the usual situation, or it could be taken as a known function of x). Thus

$$F(u) \approx A_{FI}(u) \exp [j\phi_I(u)] + j\exp [j\theta_I] \times \int_x A_I(x) \, \delta\theta(x) \exp [-jkxu] \, dx \tag{B-8}$$

where $A_{FI}(u)$ and $\phi_I(u)$ are the ideal far-field functions.

The aperture phase error can now be represented, in general, by

$$\delta\theta(x) \equiv \sum^{N} a_n g_n(x) \tag{B-9}$$

where $g_n(x)$ is the comb function and the a_n are real coefficients. Equation (B-8) can now be written

$$F(u) \approx A_{FI}(u) \exp [j\phi_I(u)] + j\exp [j\theta_I] \times \sum^{N} a_n \int_x A_I(x) g_n(x) \exp [-jkxu] \, dx \tag{B-10}$$

Equation (B-10) presents the antenna far-field function as a sum of the far-field ideal function (perfect antenna) plus the residual errors (in both amplitude and phase) introduced by the residual phase errors in the antenna aperture.

The coefficients a_n are found by minimizing the square error function E (see Appendix A) over the field of far zone positions u.

$$E = N^{-2} \sum_{u} \left\{ |A_F(u)|^2 - \left| A_{FI}(u) \exp\left[j\phi_I(u)\right] + j \exp\left[j\theta_I\right] \sum^{N} a_n \int_x A_I(x)\, g_n(x) \exp\left[-jkux\right] dx \right|^2 \right\} \tag{B-11}$$

where $|A_F(u)|^2$ is the measured antenna far-field intensity.

$$E = f(a_1, a_2, \ldots a_n) \tag{B-12}$$

The function E has a quadratic form and the minimization of Eq. (B-11) can thus be done in one step using a standard Newton-Raphson method. Note that the gradient and the Hessian matrices are readily found from the same function evaluations of

$$\int_x A_I(x)\, g_n(x) \exp\left[-jkux\right] dx$$

In essence, the solution for the unknown a_n or $\delta\theta(x)$ is found in closed form.